

## Article

# Comparative Study of Docking Tools for Evaluation of Potential Copper Metallodrugs and Their Interaction with TMPRSS2

Sergio Vázquez-Rodríguez <sup>1</sup>, Diego Ramírez-Contreras <sup>1</sup> , Lisset Noriega <sup>2</sup>, Amalia García-García <sup>1,3</sup> , Brenda L. Sánchez-Gaytán <sup>1</sup>, Francisco J. Meléndez <sup>4</sup> , Walter Filgueira de Azevedo, Jr. <sup>5</sup>, María Eugenia Castro <sup>1,\*</sup>  and Enrique González-Vergara <sup>1,\*</sup> 

<sup>1</sup> Centro de Química del Instituto de Ciencias, Benemérita Universidad Autónoma de Puebla, Puebla 72570, Mexico

<sup>2</sup> Departamento de Física Aplicada, Centro de Investigación y de Estudios Avanzados del Instituto Politécnico Nacional, Mérida 97205, Mexico; lisset.noriega@alumno.buap.mx

<sup>3</sup> Departamento de Química Inorgánica, Facultad de Ciencias, Universidad de Granada, 18012 Granada, Spain

<sup>4</sup> Laboratorio de Química Teórica, Departamento de Físicoquímica, Facultad de Ciencias Químicas, Benemérita Universidad Autónoma de Puebla, Puebla 72570, Mexico; francisco.melendez@correo.buap.mx

<sup>5</sup> Escola de Ciências da Saúde, Pontifícia Universidade Católica do Rio Grande do Sul (PUCRS), Porto Alegre 90619-900, Rio Grande do Sul, Brazil

\* Correspondence: mareug.castro@correo.buap.mx (M.E.C.); enrique.gonzalez@correo.buap.mx (E.G.-V.)

**Abstract:** COVID-19 has caused over seven million deaths globally due to its high transmission rate. The virus responsible for the disease requires a transmembrane protease serine type II (TMPRSS2-7MEQ) to infiltrate host cells and has been linked to several cancers, particularly prostate cancer. To investigate COVID-19 potential therapies, a series of Casiopeina-like copper complexes containing 1,10-Phenanthroline and amino acids were investigated as TMPRSS2 inhibitors. The molecular structures of twelve Phenanthroline copper complexes were calculated, and their global reactivity indices were analyzed using DFT and conceptual DFT methods. Three molecular docking algorithms were employed to identify the most effective inhibitors by examining their interactions with amino acid residues in the target protein's catalytic activity triad (Asp345, His296, and Ser441). All complexes are docked above the catalytic site, blocking the interaction with substrates. The Phenanthroline complexes showed better interactions than the Bipyridine complexes, likely due to increased hydrophobic contacts. Analogs' cationic nature and amino acids' basic side chains bring them near the active site by interacting with Asp435. The top complexes in this study contain Ornithine, Lysine, and Arginine, making them promising alternatives for researching new drugs for COVID-19 and cancers like prostate cancer.

**Keywords:** COVID-19; molecular docking; TMPRSS2; prostate cancer; potential copper metallodrugs; DFT calculations



**Citation:** Vázquez-Rodríguez, S.; Ramírez-Contreras, D.; Noriega, L.; García-García, A.; Sánchez-Gaytán, B.L.; Meléndez, F.J.; Filgueira de Azevedo, W., Jr.; Castro, M.E.; González-Vergara, E. Comparative Study of Docking Tools for Evaluation of Potential Copper Metallodrugs and Their Interaction with TMPRSS2. *Inorganics* **2024**, *12*, 282. <https://doi.org/10.3390/inorganics12110282>

Academic Editors: Snežana Jovanović-Stević and Jovana V. Bogojeski

Received: 29 September 2024

Revised: 24 October 2024

Accepted: 28 October 2024

Published: 30 October 2024



**Copyright:** © 2024 by the authors. Licensee MDPI, Basel, Switzerland. This article is an open access article distributed under the terms and conditions of the Creative Commons Attribution (CC BY) license (<https://creativecommons.org/licenses/by/4.0/>).

## 1. Introduction

Due to the elevated rates of infection and mortality caused by specific viral strains, there is a pressing demand for novel treatments. The trial candidates have included chemical compounds, antibodies, plasma treatment, and other options. Nevertheless, metal-based representatives have also been considered due to their unique modes of action that differ from those of organic derivatives. The initial results suggest that the development of metal-based inhibitors with improved selectivity and less toxicity is likely. This approach could be explored as an alternative method for treating upcoming virus outbreaks. This particular course is likely to require significant exertion [1].

TMPRSS2 is present in the epithelium of numerous tissues, including the prostate, gastrointestinal tract, breast, lung, kidney, pancreas, ovary, retina, respiratory tract, and salivary gland [2–6]. TMPRSS2 is upregulated in androgen-dependent prostate cancer, where

it likely mediates oncogenic activities by activating matriptase or cleaving pro-HGF [7–9]. In approximately 50% of prostate cancer cases, the TMPRSS2:ERG fusion gene initiates early transformation and sustains oncogenic and metastatic signaling [10,11]. Similar to multiple HAT/DESC family proteases, TMPRSS2 may increase virus propagation by cleaving the HA protein of influenza viruses [12,13], the SARS-CoV-1 coronavirus spike protein [14,15], and the MERS coronavirus spike protein [16,17]. Notably, TMPRSS2-deficient mice are highly resistant to experimental influenza A virus (IAV), which is associated with decreased HA cleavage in vivo, indicating that TMPRSS2 is a crucial host protease for IAV infection. Therefore, it may represent a new human therapeutic target [12,18,19]. TMPRSS2 was found to cleave the SARS-CoV-2 spike protein [20,21] and to mediate viral entry into the host cell [22], demonstrating its role in the susceptibility and tropism of SARS-CoV-2 infection [23,24]. Several studies have also identified protective and deleterious TMPRSS2 genetic variants that influence the severity of SARS-CoV-2 disease, viral burden, and the risk of infection [25,26]. As a result, inhibitors that limit proteolytic activity and anti-androgen therapies to reduce TMPRSS2 expression are being investigated as therapeutic strategies to combat the COVID-19 global pandemic [27]. The endogenous inhibition of TMPRSS2 by alpha-1 antitrypsin and HAI-2 may also attenuate infection with SARS-CoV-2 [28,29]. In addition, it is hypothesized that elevated TMPRSS2 expression in numerous malignancies, particularly prostate and colorectal, increases susceptibility to COVID-19 [6,30].

Metallo drugs, commonly used in medicine, could be promising candidates for treating COVID-19 and prostate cancer. This is primarily due to the presence of coordination compounds in metallo drugs, which possess unique reactivity features that organic chemicals alone cannot replicate [31]. Various metal ions, including iron, zinc, and copper, as well as non-metal selenium, have been identified as capable of obstructing the contact between the virus and the host cell. This obstruction prevents infection, hinders virus reproduction, disrupts viral structure, and inhibits essential enzyme function [32]. Casiopeinas<sup>®</sup> are copper(II) compounds with planar structures and ligands such as Phenanthroline or Bipyridine. Despite the significance of these chemicals in combating cancer, parasites, and germs, recent studies have focused on investigating their inhibitory impact on the principal protease, Mpro. This enzyme is responsible for the genetic material replication and initial transcription of the SARS-CoV-2 virus's genetic material. Reina [33] determined that most of the investigated Casiopeinas<sup>®</sup> had a higher level of inhibition of Mpro compared to free monochelates, bioactive ligands, and boceprevir (a well-known inhibitor).

We recently used the DFT methodology to investigate the optimized molecular structures of seven copper complexes with Bipyridine [34]. These complexes contain the amino acid residues Arg, Orn, Lys, Citr, Asn, The, and Gln, as well as two Casiopeinas, Cas III-ia and Cas IX-gly, containing acetylacetonato and Gly, respectively.

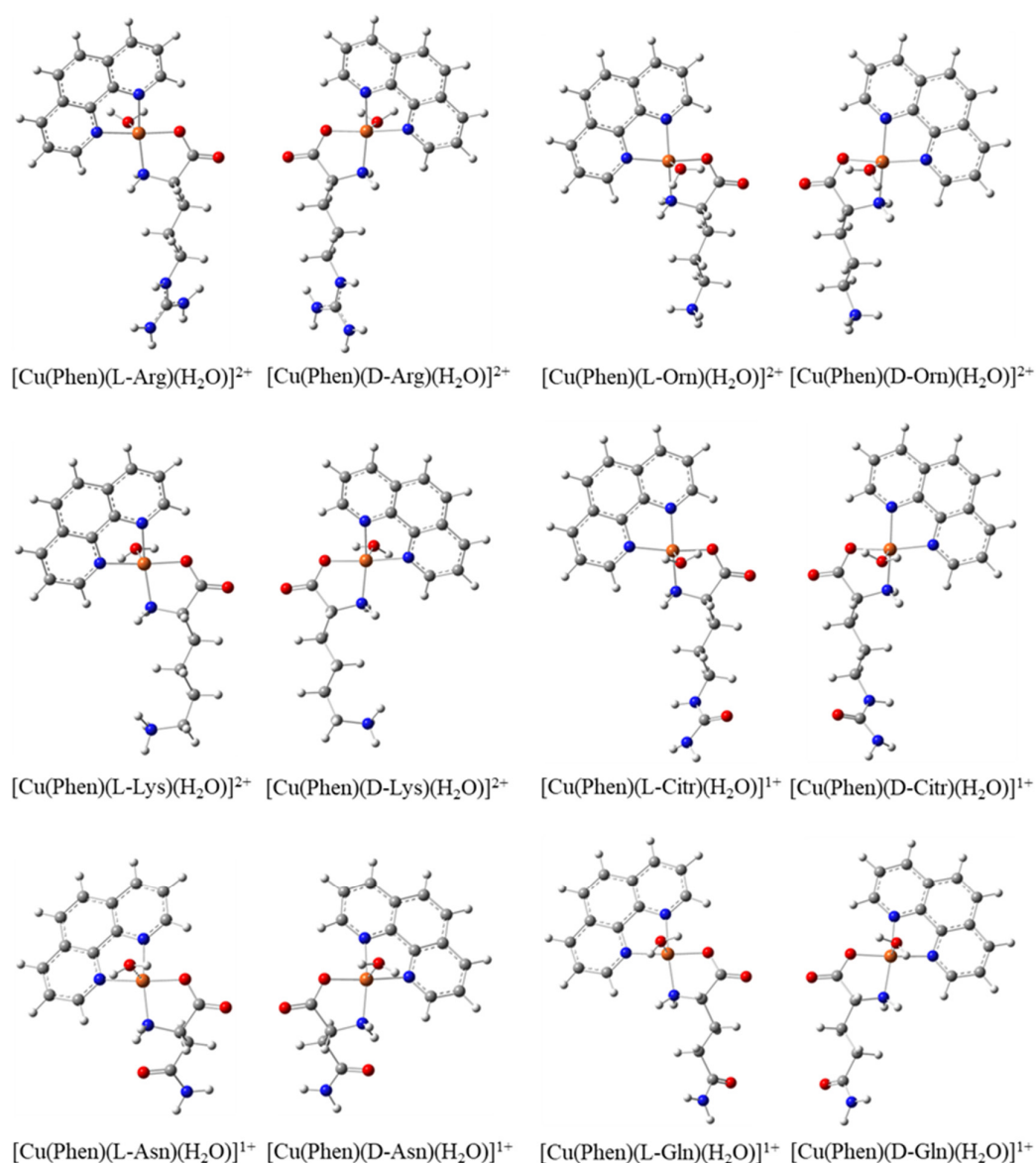
We extended our studies to twelve copper compounds using L and D-amino acidates and 1,10-Phenanthroline. Copper compounds, due to their localization just above the catalytic triad, can hinder substrate entry into a critical cavity. Their binding energies fall within the range of binding energies exhibited by other costly synthetic medicines presently available. Given that TMPRSS2 serine protease represents a promising target for inhibiting viral entry into cells and is also involved in prostate cancer, the examined complexes provide a promising starting point for identifying novel medicines to combat COVID-19 and prostate cancer.

## 2. Results

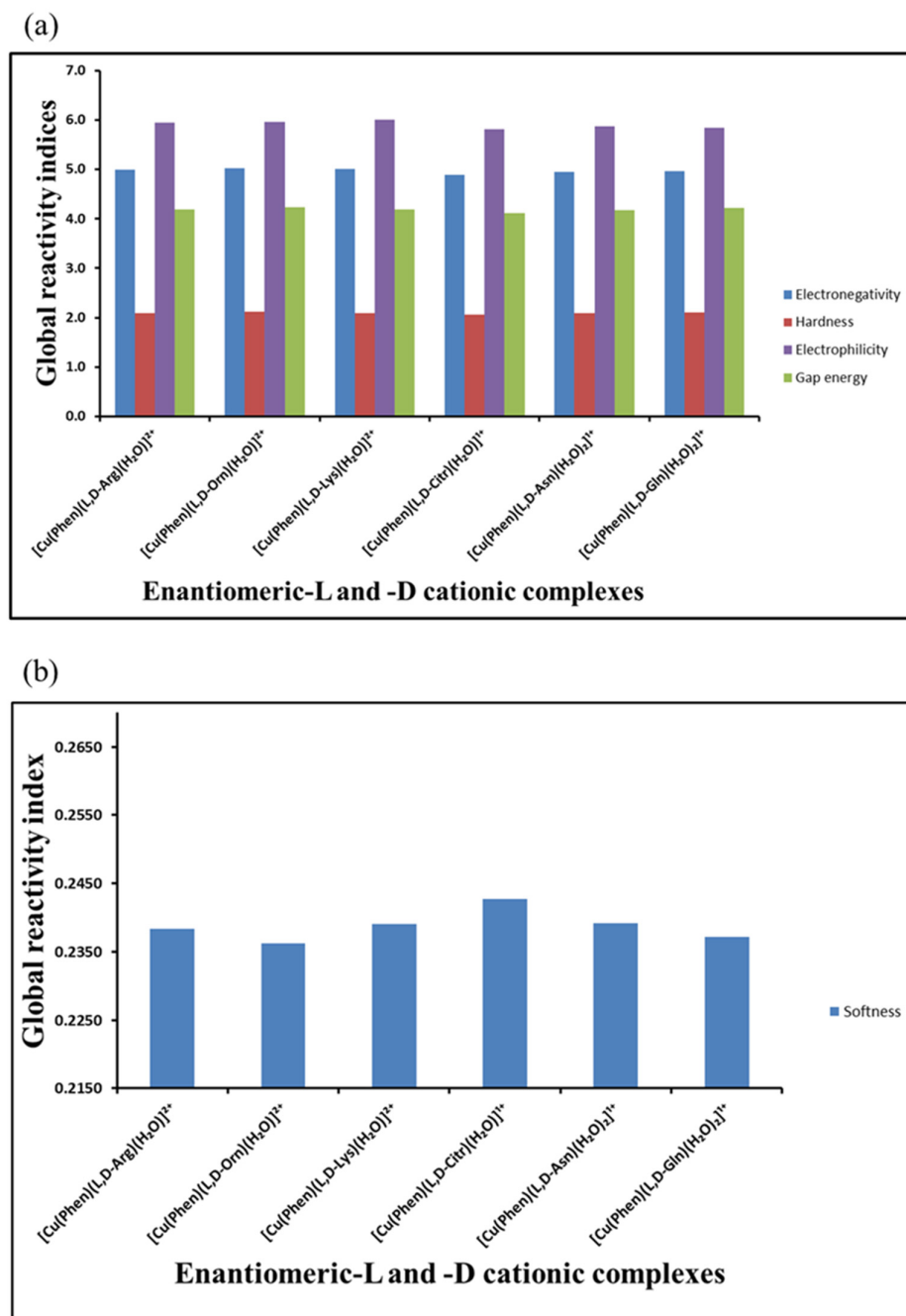
### 2.1. DFT and Conceptual DFT Calculations

Figure 1 shows the optimized molecular structures for the Phenanthroline copper complexes containing Arg, Orn, Lys, Citr, Asn, and Gln amino acid residues. All complexes contain one water molecule in the apical position of Cu(II). Table S1 shows the total electronic energies of the enantiomeric L and D-Phenanthroline copper complexes for the ground-state optimized geometry,  $E_N$ , and their ionized species,  $E_{N+1}$  and  $E_{N-1}$ . Figure 2 shows the values of the global reactivity indices. Figure 2a shows that all Phenanthroline

copper complexes present similar electronegativity values,  $\chi$ , with slightly higher values for complexes with Orn and Lys. These higher values of  $\chi$  (or lower values of chemical potential,  $\mu$ ) indicate greater resistance to electron density loss for the complexes containing Orn and Lys. The values of the electrophilicity index  $\omega$  suggest that the complexes with Arg, Orn, and Lys are slightly better electrophilic species than those with Citr, Asn, and Gln. The gap energy values,  $E_{\text{gap}}$ , show that the most reactive complex could be the complex with Citr, followed by the complexes with Asn and Lys. The values of hardness,  $\eta$ , indicate that the complexes with Orn and Gln are slightly harder, showing more resistance to exchanging their electron density with the surroundings. On the contrary, the complexes with Lys, Citr, and Asn, with the smallest  $\eta$  values (or higher values of softness,  $s$ ), can easily modify their electron density, as shown in Figure 2b. Small softness values,  $s$ , can be related to less toxicity [35].



**Figure 1.** Optimized molecular structures of the Phenanthroline copper complexes calculated with the mPW1PW91 functional in an aqueous solution. The water molecules are in the apical positions perpendicular to the plane of the paper. The structures in 2D are presented in Figure S1 in the Supplementary Materials.



**Figure 2.** (a) The reactivity global indices  $\chi$ ,  $\eta$ ,  $\omega$ , and  $E_{\text{gap}}$  and (b) the reactivity global index  $s$  of the Phenanthroline copper complexes calculated with the mPW1PW91 functional in an aqueous solution.

Compared with their analogs of the Bipyridine copper complexes with L-amino acids reported recently [34], the Phenanthroline copper complexes with L-amino acids present similar values of global reactivity indices. Phenanthroline complexes containing Arg and Orn are more reactive, with  $E_{\text{gap}}$  values slightly smaller than for the Bipyridine complexes. The complex with Arg is softer, while the complexes with Orn and Asn present similar softness to the analogs of the Bipyridine complexes. Finally, the Phenanthroline complexes with Lys, Citr, and Asn are less reactive, with higher  $E_{\text{gap}}$  values showing more stable structures. In addition, these complexes present smaller softness values,  $s$ , being less toxic than their analogs of Bipyridine, as shown in Tables S1 and S2 in the Supplementary Materials.

## 2.2. Molecular Docking Simulations

The docking simulations of the copper compounds showed that  $[\text{Cu}(\text{L-Orn})(\text{Phen})(\text{H}_2\text{O})]^{2+}$  has the lowest binding energy, determined using the MolDock Score (Table 1) (Figure 3). An examination of this ligand's docked structure (Figure 4) indicated seven hydrogen bonds, one involving a crystallographic water molecule (Wat 735 in 7MEQ). One water molecule coordinating copper in  $[\text{Cu}(\text{L-Orn})(\text{Phen})(\text{H}_2\text{O})]^{2+}$  completes the coordination sphere. Intermolecular hydrogen bonds involving the following residues of TMPRSS2 were identified: Asp 435, Ser 436, Ser 441, Gly 464, and Arg 470.

**Table 1.** Docking results for copper complexes.

Complex	AutoDock (kcal/mol)	MolDock Score (au) <sup>1</sup>	Gold
$[\text{Cu}(\text{L-Orn})(\text{Phen})(\text{H}_2\text{O})]^{+2}$	−9.1	−141.031	64.138
$[\text{Cu}(\text{L-Arg})(\text{Phen})(\text{H}_2\text{O})]^{+2}$	−7.8	−134.321	66.241
$[\text{Cu}(\text{L-Lys})(\text{Phen})(\text{H}_2\text{O})]^{+2}$	−9.3	−126.854	63.275
$[\text{Cu}(\text{D-Arg})(\text{Phen})(\text{H}_2\text{O})]^{+2}$	−9.2	−123.401	64.113
$[\text{Cu}(\text{D-Lys})(\text{Phen})(\text{H}_2\text{O})]^{+2}$	−9.1	−121.586	71.661
$[\text{Cu}(\text{L-Gln})(\text{Phen})(\text{H}_2\text{O})]^{+1}$	−7.9	−121.429	47.161
$[\text{Cu}(\text{D-Citr})(\text{phen})(\text{H}_2\text{O})]^{+1}$	−7.9	−120.582	53.645
$[\text{Cu}(\text{L-Citr})(\text{Phen})(\text{H}_2\text{O})]^{+1}$	−8.4	−118.935	66.187
$[\text{Cu}(\text{L-Asn})(\text{Phen})(\text{H}_2\text{O})]^{+1}$	−7.5	−118.920	51.913
$[\text{Cu}(\text{D-Gln})(\text{Phen})(\text{H}_2\text{O})]^{+1}$	−6.8	−118.303	57.326
$[\text{Cu}(\text{D-Orn})(\text{Phen})(\text{H}_2\text{O})]^{+1}$	−8.4	−117.966	55.284
$[\text{Cu}(\text{D-Asn})(\text{Phen})(\text{H}_2\text{O})]^{+1}$	−7.4	−112.268	52.377
GBS <sup>2</sup>	−6.3	−87.8000	46.390

<sup>1</sup> Arbitrary units (au). <sup>2</sup> Nafamostat.

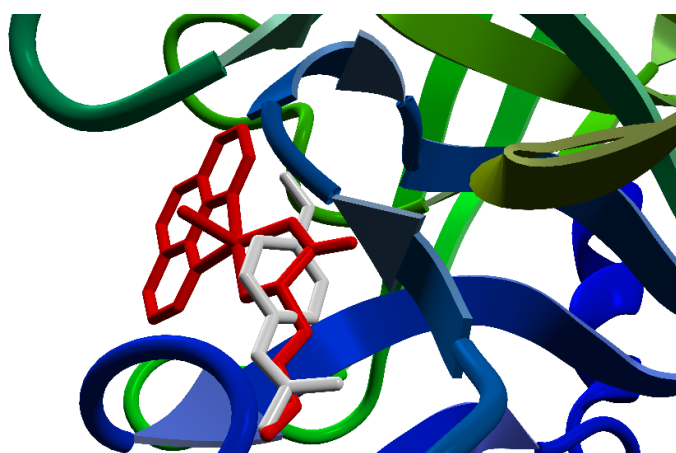


**Figure 3.** The docking results for the  $[\text{Cu}(\text{L-Orn})(\text{Phen})]$  cation (red) against the structure TM-PRSS2. In light gray, the pose for the protease inhibitor nafamostat is presented. The program Molegro < Molecular < Viewer 2.5 was used to produce this figure.

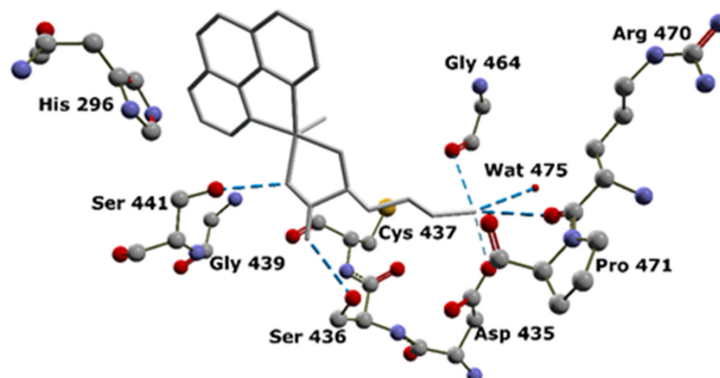


**Figure 4.** Hydrogen bonds (dashed blue lines) of the  $[\text{Cu}(\text{L-Orn})(\text{Phen})(\text{H}_2\text{O})]^{2+}$  complex and TMPRSS2. The protein atoms are indicated using a ball-and-stick representation (blue for nitrogen, gray for carbon, yellow for sulfur, and red for oxygen). The copper compound (light gray) is presented as a stick representation. Hydrogen atoms are not presented in the above figure. The program MVD was used to produce this figure.

Previous investigations of the intermolecular hydrogen bonds for the TMPRSS2–nafamostat structure revealed that the contacts with the following residues were preserved: Asp 435, Ser 436, Ser 441, and Gly 464. Analysis of TMPRSS2– $[\text{Cu}(\text{L-Orn})(\text{Phen})(\text{H}_2\text{O})]^{2+}$  indicated that the residues His 296, Cys 437, Gly 439, and Pro 471 are close to the copper compound but do not participate in the intermolecular hydrogen bonds in the complex. In a previous study [34], we identified these residues in the hydrogen bonds with the copper compound  $[\text{Cu}(\text{L-Arg})(\text{Bipy})]^{2+}$ . The structure of TMPRSS2– $[\text{Cu}(\text{L-Orn})(\text{Phen})(\text{H}_2\text{O})]^{2+}$  preserved the overall network of the intermolecular contacts observed in other inhibitors. The participation of the residue Arg 470 in hydrogen bonding is specific for most copper compounds (including  $[\text{Cu}(\text{L-Orn})(\text{Phen})(\text{H}_2\text{O})]^{2+}$ ) and is not observed in the TMPRSS2–nafamostat structure. This extra intermolecular interaction in the  $[\text{Cu}(\text{L-Orn})(\text{Phen})(\text{H}_2\text{O})]^{2+}$  complex contributed to the lowest energy calculated for this copper compound.

The low value for  $[\text{Cu}(\text{L-Arg})(\text{Phen})(\text{H}_2\text{O})]^{2+}$  in the AutoDock docking calculation could be explained by the fact that the apical water molecule points to the inside of the protein. Thus, its hydrogen bond interaction precludes the maximization of the  $\pi$ - $\pi$  and the hydrophobic interactions with the protein's surface, as seen in Figure 5.

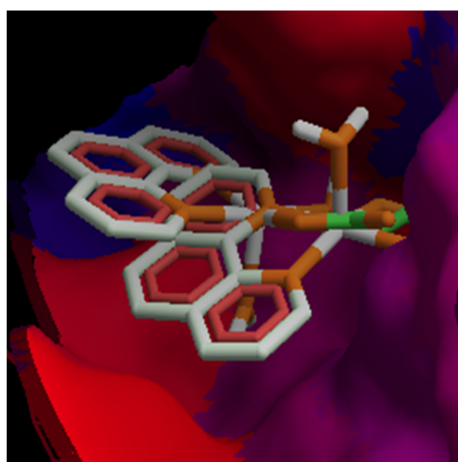


**Figure 5.** Superimposed structures of  $[\text{Cu}(\text{L-Lys})(\text{Phen})(\text{H}_2\text{O})]^{2+}$  and  $[\text{Cu}(\text{L-Arg})(\text{Phen})(\text{H}_2\text{O})]^{2+}$  on the surface of TMPRSS2 obtained through AutoDock. The coordinated water molecule pointing toward the inside of the protein, despite the hydrogen bonded to Ser441, does not allow the three Phenanthroline rings to pose flat on the surface of the protein, thus precluding strong  $\pi$ - $\pi$  interactions. The figure represents the ions landing in the hydrophobicity surface which was constructed using Molegro Molecular Viewer 2.5.

In Figures 6 and 7, superimposed structures are presented to indicate how the copper complexes interact with the surface of the protein.

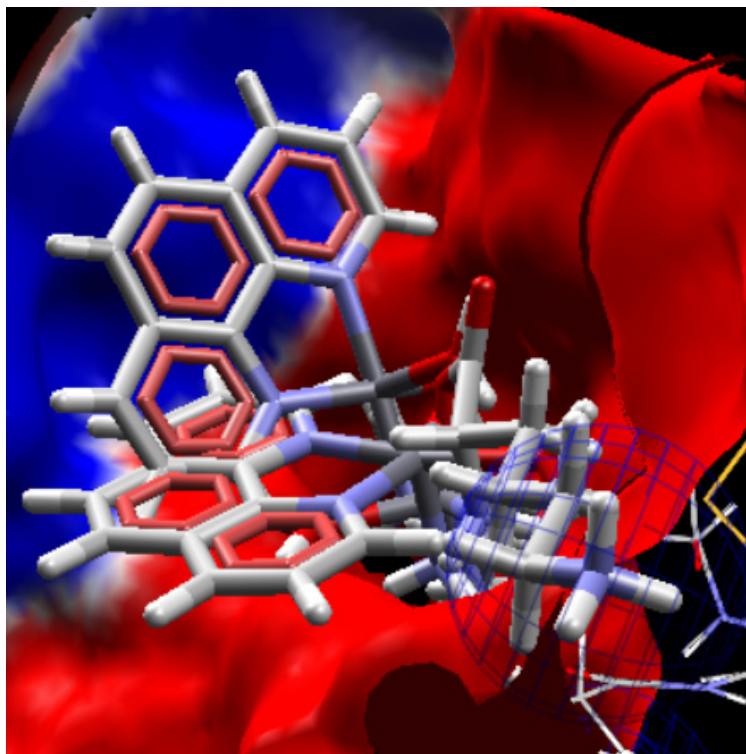


**Figure 6.** Superimposed structures of  $[\text{Cu}(\text{L-Lysine})(\text{Phen})(\text{H}_2\text{O})]^{2+}$  using the three docking programs. Although they concentrate in the channel that points to Asp435, Molegro does not introduce the lysine tail into the channel and points the tail away from it. The figure represents the electrostatic surface which was constructed by using Molegro Molecular Viewer 2.5.

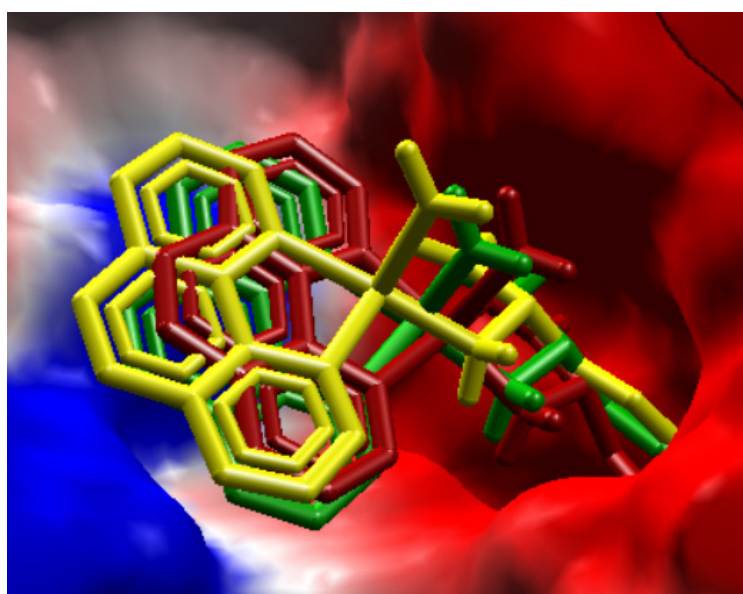


**Figure 7.** Superimposed structures of Arg (yellow), Orn (green), and Lys (red) on the surface of TMPRSS2 calculated with the GOLD program. Here, the electrostatic interaction surface is represented with a red color. The pocket at the end contains a carboxylic group of Asp435, which forms a salt bridge with the terminal amino group of lysine. The figure represents the electrostatic surface which was constructed by using Molegro Molecular Viewer 2.5.

Although AutoDock is considered a standard in docking calculations and Molegro gives good quality representations, GOLD gives us the most consistent results.

### 3. Discussion

After four years of the epidemic, COVID-19 continues to exert pressure on health-care systems, resulting in a significant global death rate. Presently, the primary focus is on antibodies, organic compounds, and previously approved medications for various diseases, including chloroquine, favipiravir, remdesivir, molnupiravir, nirmatrevir, and paxlovid [36], as well as the Mpro inhibitor currently undergoing phase III testing, S-217622 (ensitrelvir) [37]. Investigations into natural compounds have also been conducted; for instance, Manjunathan [38] studied ten bioactive substances in TMPRSS2. His results identified quercetin and genistein as potential inhibitors. The study's fundamental discoveries include the formation of hydrogen bonds on the catalytic unit of the TMPRSS2 protein and the creation of a durable protein–quercetin complex.

Owing to its significant involvement in initiating SARS-CoV-2 and other respiratory viral infections, it is hypothesized that controlling the expression or activity of TMPRSS2 is a viable focus for potential COVID-19 and prostate cancer therapies. The core functional residues of TMPRSS2 (His296, Ser441, and Ser460) engage in interactions with adjacent residues of the cleavage sites of the SARS-CoV-2 spike protein. The TMPRSS2 region interacts with the C-terminal cleavage site (Arg815/Ser816) included in the spike protein of SARS-CoV-2. The pharmacological potential of this location has been deemed higher than that of the N-terminal cleavage site (Arg685/Ser686). Hussain [39] proposes that combining human TMPRSS2 and the SARS-CoV-2 spike protein could be a promising therapeutic target for directing structure-based drug design.

Further investigation has been conducted on metal-based compounds as potential anti-SARS-CoV-2 agents [31,32,40–43]. Applying metal complexes in managing viral infections has been suggested as a therapeutic breakthrough. An illustration of this phenomenon can be seen in the research conducted by Lockwood [44]. In his comprehensive analysis of the relationship between COVID-19 and zinc, Lockwood suggests that the observed enhancement in clinical outcomes when zinc and metformin are combined in patients can be attributed primarily to creating a complex between these two compounds. This complex enhances zinc absorption and effectively functions as a non-natural protease inhibitor. Although using different pathways, Auranofin, a well-known gold compound used for rheumatoid arthritis, has been approved by the FDA as a repurposing drug for COVID-19 [45]. Auranofin acts at several levels to interfere with SARSCoV-2 entry through endocytosis and the inflammatory response, which is a source of morbidity in COVID-19. In vivo studies using animal models and clinical studies would make it possible to validate the therapeutic potential of Auranofin.

Covalent interactions between copper(II) complexes and important SARS-CoV-2 targets, including Mpro, PLpro, the spike protein, and ACE2, have been shown by molecular docking studies [46,47]. The square planar complex  $[Cu(L)_2]$ , where  $L = 2-(4\text{-morpholino benzylideneamino})phenol$  [48], exhibits a binding energy of  $-7.8$  kcal/mol against Mpro with AutoDock Vina (interactions not specified). This value falls within the binding energy range of the copper complexes with Arg, Orn, and Lys investigated in this study. Furthermore, AutoDock was used to study fifty Casiopeinas<sup>®</sup> and associated Cu(II) compounds as inhibitors of Mpro function [33]. Casiopeinas<sup>®</sup>, including CasII-5CIsa, CasII-ambz, and CasII-tyr, exhibit effective binding energies ranging from  $-8.58$  to  $-9.25$  kcal/mol, which are lower than those of boceprevir and the N3 peptide. These Casiopeinas interact with specific residues in the catalytic site cavity of Mpro, namely His41, Asn142, Cys145, Glu166, and Gln189 [49]. On the other hand, Cas III-ia and Cas IX-gly, acting as inhibitors of TMPRSS2, demonstrate binding energies ranging from  $-5.8$  to  $-7.3$  kcal/mol.

In this study, we have demonstrated that copper(II) Phenantroline complexes obtained from amino acids, which are analogs of Casiopeinas<sup>®</sup>, have promising potential as metal-lodrugs for combating COVID-19. These complexes compare favorably to Casiopeinas<sup>®</sup>,

undergoing phase I clinical trials, and to nafamostat. The cationic properties of the analogs and the basic characteristics of the amino acid side chains enable them to be anchored at the active site by interacting with Asp495. This crucial amino acid residue is fundamental for binding to arginine or lysine residues of target proteins. Given that androgens regulate TMPRSS2 and play a role in cancer metastasis [50], as well as being essential for coronavirus infection [51], copper-based inhibitors of TMPRSS2 have the potential to be used as dual-purpose treatments for both cancer and COVID-19.

#### 4. Materials and Methods

##### 4.1. DFT and Conceptual DFT Calculations

The optimized molecular structures were calculated using the functional mPW1PW91 [52] with the basis set 6-311G(d) [53] for C, N, and O atoms and 6-31G [54] for H atoms. A valence double zeta with polarization on all atoms' VDZP basis set [55] was used for the Cu atom. Vibrational frequency calculations were performed to assure true minima structures ( $\nu_i > 0$ ) at the same level of theory. The conductor-like polarizable continuum model (CPCM) [56] was used to consider the solvent's effect in aqueous solutions. The initial guess for optimization calculations of the Phenanthroline complexes was built from the crystal structures previously reported with aminoacidates of Arginine (Arg) [57], Ornithine (Orn) [58], Lysine (Lys) [59], and Citrulline (Citr) [60,61]; Asparagine (Asn) [62]; and Glutamine (Gln) [63]; or modeled from them using Spartan'20 (Wavefunction Inc., Irving, CA, USA) [64]. The global reactivity indices were calculated using the vertical Self-Consistent Field ( $\Delta$ SCF) approach [65]. In this approach, the vertical ionization potential (I) and the vertical electron affinity (A) were obtained from the ground-state geometry. Their corresponding ionized species are  $I = E_{N+1} - E_N$  and  $A = E_N - E_{N-1}$ , where  $E_N$  is the electronic energy of the ground state and  $E_{N+1}$  and  $E_{N-1}$  are the electronic energies of the system with one less electron and one more electron, respectively, according to the  $\Delta$ SCF approach. The global reactivity indices, such as the chemical potential ( $\mu$ ), electronegativity ( $\chi$ ), hardness ( $\eta$ ), softness ( $s$ ), and electrophilicity index ( $\omega$ ), were obtained with the following equations:  $\mu = -(I + A)/2$ ;  $\chi = (I + A)/2$ ;  $\eta = (I - A)/2$ ;  $s = 1/2\eta$ ;  $\omega = \mu^2/2\eta$ ; and  $E_{\text{gap}} = I - A$ . The global reactivity indices are compared with those obtained for their analogs of the Bipyridine copper complexes [34]. All calculations were carried out in the Gaussian 16 program package [66].

##### 4.2. Docking Studies with AutoDock4

The docking process consists of two key steps: the first is related to the conformation of the coordination complex and its orientation to the protein binding site; the second essential step consists of predicting the affinity of the complex to the protein using a scoring function. The Lamarckian genetic algorithm was used to make a random search of the conformation of the copper complexes. This algorithm considers the different complex poses and then interchanges between them, leading to a new generation of structures. Each generation member is evaluated with the scoring function, and only those values that meet the requirements (conformation, rotation, and orientation concerning the protein) continue to the next generation until the best ligand conformations are found [67]. The force field used in AutoDock4 is a semiempirical free energy scoring function that considers the contribution of the hydrogen bonds and the electrostatic interactions. This scoring function discriminates the suitable poses from the wrong ones and estimates the affinity between the complexes and the protein. The protein and complexes were prepared through AutoDockTools4 by removing water molecules and polar hydrogens and adding Gasteiger charges. The receptor grid box was centered at  $x = 9.3$ ,  $y = -5.9$ , and  $z = -19.993$  Å. The box size was  $40$  Å<sup>3</sup>. Docking studies were conducted with 150 individuals in the population, with a maximum energy evaluation of 2,500,000 and a maximum generation of 27,000, resulting in 50 docking poses. The parameters for the copper(II) atom were the sum of the Van der Waals radii of two similar atoms ( $3.50$  Å), the Van der Waals well depth ( $0.005$  kmol mol<sup>-1</sup>), the atomic solvation volume ( $12.0$  Å<sup>3</sup>), and the atomic solvation pa-

parameter ( $-0.00110$ ). The hydrogen bond radius of the heteroatom in contact with hydrogen ( $0.0 \text{ \AA}$ ), the well depth of the hydrogen bond ( $0.0 \text{ kcal mol}^{-1}$ ), and various integers indicate the type of hydrogen bonding atom and the indexes for the generation of the autogrid map ( $0, -1, -1, 1$ , respectively).

#### 4.3. Docking Simulations with Molegro Virtual Docker

In this study, we applied a previously described docking protocol [34] using the Molegro Virtual Docker (MVD, Molexus, Odder, Denmark) [68]. Briefly, we utilized the MVD to assess the intermolecular interactions of the copper compounds against the structure of transmembrane protease serine 2 (TMPRSS2) (PDB: 7MEQ) [69]. Function "Reduce" [70] added hydrogens to the protein structure file. The MVD added atomic charges to all ligands and proteins for the docking simulations [71]. We used Ant Colony Optimization [72] and the MolDock scoring function [68,73] for the docking simulations. After the docking simulations, all structures underwent energy minimization using the Nelder–Mead algorithm [74] implemented in the MVD. For all docking simulations, we removed the coordinates of the 7MEQ inhibitor nafamostat.

#### 4.4. Docking Studies with GOLD (Genetic Optimization for Ligand Docking)

The Goldscore function is a scoring function used to rank different ways of binding. It is based on molecular mechanics and consists of four terms:

$$\text{GOLD Fitness} = \text{Shb\_ext} + \text{Svdw\_ext} + \text{Shb\_int} + \text{Svdw\_int} \quad (1)$$

Shb\_ext is the hydrogen bond score between the protein and complex, and Svdw\_ext is the Van der Waals score between them. Shb\_int is the contribution to fitness from the intramolecular hydrogen bonds in the complex. This term is turned off in all calculations [75] (this is the GOLD default and usually gives the best results). Svdw\_int represents the intramolecular strain's contribution to the complex. GOLD (version 2023.2, provided by CCDC, Cambridge, UK) uses a genetic algorithm (GA) to change or improve parameters such as rotatable bonds, ring geometries, protein groups, and binding sites. The Hermes software was used to carry out the protein preparation, which included removing water molecules before adding polar hydrogens and removing the nafamostat inhibitor. For the simulation, a maximum of 125,000 GA operations were carried out on a single population of 100 GA runs for each of the ten independent GA runs. Crossover, mutation, and migration operator weights were left at their default values. The docking study was performed in the area comprising the active sites and the closest residues and was constricted to a  $10 \text{ \AA}$  radius sphere centered at the coordinates  $x = -6.04$ ,  $y = -3.15$ , and  $z = 15.65 \text{ \AA}$ .

## 5. Conclusions

The molecular structures of twelve Phenanthroline copper complexes were calculated, and their global reactivity indices were analyzed using DFT and conceptual DFT methods to predict their pharmacological activity. The DFT results generally showed values for the global reactivity indices of the Phenanthroline complexes similar to those of the Bipyridine complexes. However, the Phenanthroline complexes presented smaller softness values, indicating less toxicity than their analogs of Bipyridine and, therefore, better pharmacological activity. For the studied complexes, the binding energy/docking score is better than for the nafamostat inhibitor (GBS) and tested Casiopeina complexes. The Phenanthroline complexes show better interactions than the Bipyridine complexes (as previously reported), likely due to increased hydrophobic contacts. The number of hydrogen bonds and the presence of a salt bridge (involving terminal nitrogen atoms and Asp435) increase the protein complexes' stability. The copper compounds localize just above the catalytic triad to stop substrates from entering into it. The low value for Arginine in the AutoDock docking calculation could be explained by the fact that the apical water molecule points to the inside of the protein. Thus, its hydrogen bond interaction precludes the maximization of the  $\pi$ - $\pi$  and hydrophobic interactions with the protein's surface.

Because serine protease could be an excellent target to stop the virus from entering into the cell, the analyzed complexes are an excellent place to start looking for new drugs to treat COVID-19 and prostate cancer. Additional research will lead to metal-based inhibitors with enhanced selectivity and reduced toxicity, which could be considered an alternative strategy for treating future viral outbreaks and cancers where TMPRSS2 is an important player.

**Supplementary Materials:** The following supporting information can be downloaded at <https://www.mdpi.com/article/10.3390/inorganics12110282/s1>, Figure S1. D complexes (left) and L complexes (Right). (A)  $[\text{Cu}(\text{Lys})(\text{Phen})(\text{H}_2\text{O})]^{+2}$ ; (B)  $[\text{Cu}(\text{Orn})(\text{Phen})(\text{H}_2\text{O})]^{+2}$ ; (C)  $[\text{Cu}(\text{Gln})(\text{Phen})(\text{H}_2\text{O})]^{+1}$ ; (D)  $[\text{Cu}(\text{Arg})(\text{Phen})(\text{H}_2\text{O})]^{+2}$ ; (E)  $[\text{Cu}(\text{Cit})(\text{phen})(\text{H}_2\text{O})]^{+1}$ ; and (F)  $[\text{Cu}(\text{Asn})(\text{Phen})(\text{H}_2\text{O})]^{+1}$ . Table S1. Energies in a.u. of the enantiomeric L and D copper complexes calculated with the mPW1PW91 functional in aqueous solutions. Table S2. The global reactivity indices of the enantiomeric-L and -D copper complexes calculated with the mPW1PW91 functional in aqueous solutions, all in eV units: vertical ionization potential (I), vertical electron affinity (A), gap energy (E<sub>gap</sub>), chemical potential (μ), electronegativity (χ), hardness (η), softness (s), and electrophilicity index (ω).

**Author Contributions:** S.V.-R., D.R.-C., L.N. and W.F.d.A.J. conducted the docking simulations. F.J.M. and M.E.C. carried out the DFT calculations. S.V.-R., D.R.-C., L.N., E.G.-V., M.E.C., A.G.-G. and B.L.S.-G. wrote and revised the manuscript. S.V.-R., D.R.-C. and E.G.-V. conceived and designed this study. All authors contributed extensively to the work presented in this paper. All authors have read and agreed to the published version of the manuscript.

**Funding:** Projects which funded this research include 100108444-VIEP, 100256733-VIEP, and 100233622-VIEP; the PRODEP Academic Group BUAP-CA-263 (SEP, Mexico); and the Ministerio de Universidades and Next-Generation Funds for the Margarita Salas contract 401 (Spain). This work was also supported by a grant from CNPq (Brazil) (309029/2018-0).

**Data Availability Statement:** The raw data supporting the conclusions of this article will be made available by the authors on request.

**Acknowledgments:** S.V.-R., D.R.-C., and L.N. thank CONACyT for their M.Sc. and Ph.D. fellowship support numbers 1143792 and 774653 and postdoctoral fellowship. M.C. and F.M. wish to thank the Laboratorio Nacional de Supercómputo del Sureste de México (LNS-BUAP) and the CONACyT network of national laboratories for the computer resources and support provided. A.G.-G. thanks the Ministerio de Universidades and its funding via Next-Generation Funds (Spain).

**Conflicts of Interest:** The authors declare no conflicts of interest.

## References

1. Mehrotra, R.; Shukla, S.N.; Gaur, P. Metallo-Antiviral Aspirants: Answer to the Upcoming Virus Outbreak. *Eur. J. Med. Chem. Rep.* **2020**, *8*, 100104. [[CrossRef](#)] [[PubMed](#)]
2. Faller, N.; Gautschi, I.; Schild, L. Functional Analysis of a Missense Mutation in the Serine Protease Inhibitor SPINT2 Associated with Congenital Sodium Diarrhea. *PLoS ONE* **2014**, *9*, e94267. [[CrossRef](#)]
3. Jacquinet, E.; Rao, N.V.; Rao, G.V.; Zhengming, W.; Albertine, K.H.; Hoidal, J.R. Cloning and Characterization of the CDNA and Gene for Human Epitheliasin. *Eur. J. Biochem.* **2001**, *268*, 2687–2699. [[CrossRef](#)]
4. Zhou, J.; Choi, S.; Liu, H.; Zhang, J.; Tian, Y.; Edlow, A.G.; Ezashi, T.; Roberts, R.M.; Ma, W.; Schust, D.J. Is SARS-CoV-2 Infection a Risk Factor for Early Pregnancy Loss? ACE2 and TMPRSS2 Coexpression and Persistent Replicative Infection in Primitive Trophoblast. *J. Infect. Dis.* **2021**, *224*, S660–S669. [[CrossRef](#)]
5. Klingenstein, M.; Klingenstein, S.; Neckel, P.H.; Mack, A.F.; Wagner, A.P.; Kleger, A.; Liebau, S.; Milazzo, A. Evidence of SARS-CoV2 Entry Protein ACE2 in the Human Nose and Olfactory Bulb. *Cells Tissues Organs* **2021**, *209*, 155–164. [[CrossRef](#)]
6. Liu, C.; Wang, K.; Zhang, M.; Hu, X.; Hu, T.; Liu, Y.; Hu, Q.; Wu, S.; Yue, J. High Expression of ACE2 and TMPRSS2 and Clinical Characteristics of COVID-19 in Colorectal Cancer Patients. *NPJ Precis. Oncol.* **2021**, *5*, 1. [[CrossRef](#)]
7. Ko, C.J.; Huang, C.C.; Lin, H.Y.; Juan, C.P.; Lan, S.W.; Shyu, H.Y.; Wu, S.R.; Hsiao, P.W.; Huang, H.P.; Shun, C.T.; et al. Androgen-Induced TMPRSS2 Activates Matriptase and Promotes Extracellular Matrix Degradation, Prostate Cancer Cell Invasion, Tumor Growth, and Metastasis. *Cancer Res.* **2015**, *75*, 2949–2960. [[CrossRef](#)]
8. Tanabe, L.M.; List, K. The Role of Type II Transmembrane Serine Protease-Mediated Signaling in Cancer. *FEBS J.* **2017**, *284*, 1421–1436. [[CrossRef](#)]
9. Pawar, N.R.; Buzza, M.S.; Antalis, T.M. Membrane-Anchored Serine Proteases and Protease-Activated Receptor-2-Mediated Signaling: Co-Conspirators in Cancer Progression. *Cancer Res.* **2019**, *79*, 301–310. [[CrossRef](#)]

10. Tomlins, S.A.; Laxman, B.; Varambally, S.; Cao, X.; Yu, J.; Helgeson, B.E.; Cao, Q.; Prensner, J.R.; Rubin, M.A.; Shah, R.B.; et al. Role of the TMPRSS2-ERG Gene Fusion in Prostate Cancer. *Neoplasia* **2008**, *10*, 177–188. [[CrossRef](#)]
11. Selvaraj, N.; Budka, J.A.; Ferris, M.W.; Jerde, T.J.; Hollenhorst, P.C. Prostate Cancer ETS Rearrangements Switch a Cell Migration Gene Expression Program from RAS/ERK to PI3K/AKT Regulation. *Mol. Cancer* **2014**, *13*, 61. [[CrossRef](#)] [[PubMed](#)]
12. Sakai, K.; Ami, Y.; Tahara, M.; Kubota, T.; Anraku, M.; Abe, M.; Nakajima, N.; Sekizuka, T.; Shirato, K.; Suzaki, Y.; et al. The Host Protease TMPRSS2 Plays a Major Role in In Vivo Replication of Emerging H7N9 and Seasonal Influenza Viruses. *J. Virol.* **2014**, *88*, 5608–5616. [[CrossRef](#)]
13. Limburg, H.; Harbig, A.; Bestle, D.; Stein, D.A.; Moulton, H.M.; Jaeger, J.; Janga, H.; Harges, K.; Koepke, J.; Schulte, L.; et al. TMPRSS2 Is the Major Activating Protease of Influenza A Virus in Primary Human Airway Cells and Influenza B Virus in Human Type II Pneumocytes. *J. Virol.* **2019**, *93*. [[CrossRef](#)]
14. Reinke, L.M.; Spiegel, M.; Plegge, T.; Hartleib, A.; Nehlmeier, I.; Gierer, S.; Hoffmann, M.; Hofmann-Winkler, H.; Winkler, M.; Pöhlmann, S. Different Residues in the SARS-CoV Spike Protein Determine Cleavage and Activation by the Host Cell Protease TMPRSS2. *PLoS ONE* **2017**, *12*, e0179177. [[CrossRef](#)]
15. Heurich, A.; Hofmann-Winkler, H.; Gierer, S.; Liepold, T.; Jahn, O.; Pöhlmann, S. TMPRSS2 and ADAM17 Cleave ACE2 Differentially and Only Proteolysis by TMPRSS2 Augments Entry Driven by the Severe Acute Respiratory Syndrome Coronavirus Spike Protein. *J. Virol.* **2014**, *88*, 1293–1307. [[CrossRef](#)]
16. Kleine-Weber, H.; Elzayat, M.T.; Hoffmann, M.; Pöhlmann, S. Functional Analysis of Potential Cleavage Sites in the MERS-Coronavirus Spike Protein. *Sci. Rep.* **2018**, *8*, 16597. [[CrossRef](#)]
17. Iwata-Yoshikawa, N.; Okamura, T.; Shimizu, Y.; Hasegawa, H.; Takeda, M.; Nagata, N.; Gallagher, T. TMPRSS2 Contributes to Virus Spread and Immunopathology in the Airways of Murine Models after Coronavirus Infection. *J. Virol.* **2019**, *93*, 1815–1833. [[CrossRef](#)]
18. Hatesuer, B.; Bertram, S.; Mehnert, N.; Bahgat, M.M.; Nelson, P.S.; Pöhlman, S.; Schughart, K. Tmprss2 Is Essential for Influenza H1N1 Virus Pathogenesis in Mice. *PLoS Pathog.* **2013**, *9*, e1003774. [[CrossRef](#)]
19. Lambert, R.L.O.; Gerhauser, I.; Nehlmeier, I.; Leist, S.R.; Kollmus, H.; Pöhlmann, S.; Schughart, K. Tmprss2 Knock-out Mice Are Resistant to H1N1 Influenza a Virus Pathogenesis. *J. Gen. Virol.* **2019**, *100*, 1073–1078. [[CrossRef](#)]
20. Bestle, D.; Heindl, M.R.; Limburg, H.; van Lam van, T.; Pilgram, O.; Moulton, H.; Stein, D.A.; Harges, K.; Eickmann, M.; Dolnik, O.; et al. TMPRSS2 and Furin Are Both Essential for Proteolytic Activation of SARS-CoV-2 in Human Airway Cells. *Life Sci. Alliance* **2020**, *3*, e202000786. [[CrossRef](#)]
21. Hoffmann, M.; Kleine-Weber, H.; Krüger, N.; Müller, M.; Drosten, C.; Pöhlmann, S. The novel coronavirus 2019 (2019-nCoV) uses the SARS-coronavirus receptor ACE2 and the Cellular Protease TMPRSS2 for Entry into Target Cells. *bioRxiv* **2020**. [[CrossRef](#)]
22. Koch, J.; Uckele, Z.M.; Doldan, P.; Stanifer, M.; Boulant, S.; Lozach, P. TMPRSS2 Expression Dictates the Entry Route Used by SARS-CoV-2 to Infect Host Cells. *EMBO J.* **2021**, *40*, e107821. [[CrossRef](#)]
23. Abbasi, A.Z.; Kiyani, D.A.; Hamid, S.M.; Saalim, M.; Fahim, A.; Jalal, N. Spiking Dependence of SARS-CoV-2 Pathogenicity on TMPRSS2. *J. Med. Virol.* **2021**, *93*, 4205–4218. [[CrossRef](#)]
24. Zhang, F.; Li, W.; Feng, J.; Ramos da Silva, S.; Ju, E.; Zhang, H.; Chang, Y.; Moore, P.S.; Guo, H.; Gao, S.J. SARS-CoV-2 Pseudovirus Infectivity and Expression of Viral Entry-Related Factors ACE2, TMPRSS2, Kim-1, and NRP-1 in Human Cells from the Respiratory, Urinary, Digestive, Reproductive, and Immune Systems. *J. Med. Virol.* **2021**, *93*, 6671–6685. [[CrossRef](#)]
25. Monticelli, M.; Mele, B.H.; Benetti, E.; Fallerini, C.; Baldassarri, M.; Furini, S.; Frullanti, E.; Mari, F.; Andreotti, G.; Cubellis, M.V.; et al. Protective Role of a Tmprss2 Variant on Severe COVID-19 Outcome in Young Males and Elderly Women. *Genes* **2021**, *12*, 596. [[CrossRef](#)]
26. Ravikanth, V.; Sasikala, M.; Naveen, V.; Latha, S.S.; Parsa, K.V.L.; Vijayasathy, K.; Amanchy, R.; Avanthi, S.; Govardhan, B.; Rakesh, K.; et al. A Variant in TMPRSS2 Is Associated with Decreased Disease Severity in COVID-19. *Meta Gene* **2021**, *29*, 100930. [[CrossRef](#)]
27. Ayele, A.G.; Enyew, E.F.; Kifle, Z.D. Roles of Existing Drug and Drug Targets for COVID-19 Management. *Metabol. Open* **2021**, *11*, 100103. [[CrossRef](#)]
28. Azouz, N.P.; Klingler, A.M.; Callahan, V.; Akhrymuk, I.V.; Elez, K.; Raich, L.; Henry, B.M.; Benoit, J.L.; Benoit, S.W.; Noé, F.; et al. Alpha 1 Antitrypsin Is an Inhibitor of the Sars-Cov-2–Priming Protease Tmprss2. *Pathog. Immun.* **2021**, *6*, 55–74. [[CrossRef](#)]
29. Tomita, Y.; Matsuyama, S.; Fukuhara, H.; Maenaka, K.; Kataoka, H.; Hashiguchi, T.; Takeda, M. The Physiological TMPRSS2 Inhibitor HAI-2 Alleviates SARS-CoV-2 Infection. *J. Virol.* **2021**, *95*. [[CrossRef](#)]
30. Sinha, S.; Kundu, C.N. Cancer and COVID-19: Why Are Cancer Patients More Susceptible to COVID-19? *Med. Oncol.* **2021**, *38*, 101. [[CrossRef](#)]
31. Cirri, D.; Pratesi, A.; Marzo, T.; Messori, L. Metallo Therapeutics for COVID-19. Exploiting Metal-Based Compounds for the Discovery of New Antiviral Drugs. *Expert. Opin. Drug Discov.* **2021**, *16*, 39–46. [[CrossRef](#)] [[PubMed](#)]
32. Ni, Y.Q.; Zeng, H.H.; Song, X.W.; Zheng, J.; Wu, H.Q.; Liu, C.T.; Zhang, Y. Potential Metal-Related Strategies for Prevention and Treatment of COVID-19. *Rare Met.* **2022**, *41*, 1129–1141. [[CrossRef](#)]
33. Reina, M.; Talavera-Contreras, L.G.; Figueroa-DePaz, Y.; Ruiz-Azuara, L.; Hernández-Ayala, L.F. Casiopeinas® as SARS-CoV-2 Main Protease (M pro) Inhibitors: A Combined DFT, Molecular Docking and ONIOM Approach. *New J. Chem.* **2022**, *46*, 12500–12511. [[CrossRef](#)]

34. Vazquez-Rodriguez, S.; Ramírez-Contreras, D.; Noriega, L.; García-García, A.; Sánchez-Gaytán, B.L.; Melendez, F.J.; Castro, M.E.; de Azevedo, W.F.; González-Vergara, E. Interaction of Copper Potential Metallo drugs with TMPRSS2: A Comparative Study of Docking Tools and Its Implications on COVID-19. *Front. Chem.* **2023**, *11*, 1128859. [CrossRef] [PubMed]
35. Siddiqui, N.; Javed, S. Quantum Computational, Spectroscopic Investigations on Ampyra (4-Aminopyridine) by Dft/Td-Dft with Different Solvents and Molecular Docking Studies. *J. Mol. Struct.* **2021**, *1224*, 129021. [CrossRef]
36. Jawaid Akhtar, M. COVID-19 Inhibitors: A Prospective Therapeutics. *Bioorg. Chem.* **2020**, *101*, 104027. [CrossRef]
37. Sasaki, M.; Tabata, K.; Kishimoto, M.; Itakura, Y.; Kobayashi, H.; Ariizumi, T.; Uemura, K.; Toba, S.; Kusakabe, S.; Maruyama, Y.; et al. S-217622, a SARS-CoV-2 Main Protease Inhibitor, Decreases Viral Load and Ameliorates COVID-19 Severity in Hamsters. *Sci. Transl. Med.* **2022**, *15*, eabq4064. [CrossRef]
38. Manjunathan, R.; Periyaswami, V.; Mitra, K.; Rosita, A.S.; Pandya, M.; Selvaraj, J.; Ravi, L.; Devarajan, N.; Doble, M. Molecular Docking Analysis Reveals the Functional Inhibitory Effect of Genistein and Quercetin on TMPRSS2: SARS-COV-2 Cell Entry Facilitator Spike Protein. *BMC Bioinform.* **2022**, *23*, 180. [CrossRef]
39. Hussain, M.; Jabeen, N.; Amanullah, A.; Baig, A.A.; Aziz, B.; Shabbir, S.; Raza, F.; Uddin, N. Molecular Docking between Human TmpRSS2 and SARS-CoV-2 Spike Protein: Conformation and Intermolecular Interactions. *AIMS Microbiol.* **2020**, *6*, 350–360. [CrossRef]
40. Karges, J.; Cohen, S.M. Metal Complexes as Antiviral Agents for SARS-CoV-2. *ChemBioChem* **2021**, *22*, 2600–2607. [CrossRef]
41. Gil-Moles, M.; Basu, U.; Büssing, R.; Hoffmeister, H.; Türck, S.; Varchmin, A.; Ott, I. Gold Metallo drugs to Target Coronavirus Proteins: Inhibitory Effects on the Spike-ACE2 Interaction and on PLpro Protease Activity by Auranofin and Gold Organometallics. *Chem.—A Eur. J.* **2020**, *26*, 15140–15144. [CrossRef] [PubMed]
42. Li, H.; Yuan, S.; Wei, X.; Sun, H. Metal-Based Strategies for the Fight against COVID-19. *Chem. Comm.* **2022**, *58*, 7466–7482. [CrossRef] [PubMed]
43. Vlasious, M.C.; Pafti, K.S. Screening Possible Drug Molecules for Covid-19. The Example of Vanadium (III/IV/V) Complex Molecules with Computational Chemistry and Molecular Docking. *Comput. Toxicol.* **2021**, *18*, 100157. [CrossRef]
44. Lockwood, T.D. Coordination Chemistry Suggests That Independently Observed Benefits of Metformin and Zn<sup>2+</sup> against COVID-19 Are Not Independent. *BioMetals* **2024**, *37*, 983–1022. [CrossRef]
45. Laplantine, E.; Chable-Bessia, C.; Oudin, A.; Swain, J.; Soria, A.; Merida, P.; Gourdelier, M.; Mestiri, S.; Besseghe, I.; Bremaud, E.; et al. The FDA-Approved Drug Auranofin Has a Dual Inhibitory Effect on SARS-CoV-2 Entry and NF-KB Signaling. *iScience* **2022**, *25*, 105066. [CrossRef]
46. Muhammad, N.; Khan, I.N.; Ali, Z.; Ibrahim, M.; Shujah, S.; Ali, S.; Ikram, M.; Rehman, S.; Khan, G.S.; Wadood, A.; et al. Synthesis, Characterization, Antioxidant, Antileishmanial, Anticancer, DNA and Theoretical SARS-CoV-2 Interaction Studies of Copper(II) Carboxylate Complexes. *J. Mol. Struct.* **2022**, *1253*, 132308. [CrossRef]
47. Al-Harbi, S.A. Synthesis and Characterization of Violurate-Based Mn(II) and Cu(II) Complexes Nano-Crystallites as DNA-Binders and Therapeutics Agents against SARS-CoV-2 Virus. *J. Saudi Chem. Soc.* **2022**, *26*, 101528. [CrossRef]
48. Sakthikumar, K.; Krause, R.W.M.; Isamura, B.K.; Raja, J.D.; Athimoolam, S. Spectro-Electrochemical, Fluorometric and Biothermodynamic Evaluation of Pharmacologically Active Morpholine Scaffold Single Crystal Ligand and Its Metal (II) Complexes: A Comparative Study on in-Vitro and in-Silico Screening towards DNA/BSA/SARS-CoV-19. *J. Inorg. Biochem.* **2022**, *236*, 111953. [CrossRef]
49. Kneller, D.W.; Phillips, G.; O'Neill, H.M.; Jedrzejczak, R.; Stols, L.; Langan, P.; Joachimiak, A.; Coates, L.; Kovalevsky, A. Structural Plasticity of SARS-CoV-2 3CL Mpro Active Site Cavity Revealed by Room Temperature X-Ray Crystallography. *Nat. Commun.* **2020**, *11*, 3202. [CrossRef]
50. Lucas, J.M.; Heinlein, C.; Kim, T.; Hernandez, S.A.; Malik, M.S.; True, L.D.; Morrissey, C.; Corey, E.; Montgomery, B.; Mostaghel, E.; et al. The Androgen-Regulated Protease TMPRSS2 Activates a Proteolytic Cascade Involving Components of the Tumor Microenvironment and Promotes Prostate Cancer Metastasis. *Cancer Discov.* **2014**, *4*, 1310–1325. [CrossRef]
51. Stopsack, K.H.; Mucci, L.A.; Antonarakis, E.S.; Nelson, P.S.; Kantoff, P.W. TMPRSS2 and COVID-19: Serendipity or Opportunity for Intervention? *Cancer Discov.* **2020**, *10*, 779–782. [CrossRef] [PubMed]
52. Adamo, C.; Barone, V. Exchange Functionals with Improved Long-Range Behavior and Adiabatic Connection Methods without Adjustable Parameters: The MPW and MPW1PW Models. *J. Chem. Phys.* **1998**, *108*, 664–675. [CrossRef]
53. Krishnan, R.; Binkley, J.S.; Seeger, R.; Pople, J.A. Self-consistent Molecular Orbital Methods. XX. A Basis Set for Correlated Wave Functions. *J. Chem. Phys.* **1980**, *72*, 650–654. [CrossRef]
54. Ditchfield, R.; Hehre, W.J.; Pople, J.A. Self-consistent Molecular-orbital Methods. IX. An Extended Gaussian-type Basis for Molecular-orbital Studies of Organic Molecules. *J. Chem. Phys.* **1971**, *54*, 724–728. [CrossRef]
55. Wachters, A.J.H. Gaussian Basis Set for Molecular Wavefunctions Containing Third-row Atoms. *J. Chem. Phys.* **1970**, *52*, 1033–1036. [CrossRef]
56. Cossi, M.; Rega, N.; Scalmani, G.; Barone, V. Energies, Structures, and Electronic Properties of Molecules in Solution with the C-PCM Solvation Model. *J. Comput. Chem.* **2003**, *24*, 669–681. [CrossRef]
57. Patra, A.K.; Bhowmick, T.; Roy, S.; Ramakumar, S.; Chakravarty, A.R. Copper(II) Complexes of L-Arginine as Netropsin Mimics Showing DNA Cleavage Activity in Red Light. *Inorg. Chem.* **2009**, *48*, 2932–2943. [CrossRef]
58. Sánchez-Lara, E.; García-García, A.; González-Vergara, E.; Cepeda, J.; Rodríguez-Diéguez, A. Magneto-Structural Correlations of Cyclo-Tetranavanadates Functionalized with Mixed-Ligand Copper(II) Complexes. *New J. Chem.* **2021**, *45*, 5081–5092. [CrossRef]

59. Martínez-Valencia, B.; Corona-Motolinia, N.D.; Sánchez-Lara, E.; Noriega, L.; Sánchez-Gaytán, B.L.; Castro, M.E.; Meléndez-Bustamante, F.; González-Vergara, E. Cyclo-Tetranadate Bridged Copper Complexes as Potential Double Bullet pro-Metallo-drugs for Cancer Treatment. *J. Inorg. Biochem.* **2020**, *208*, 111081. [[CrossRef](#)]
60. Ramírez-Contreras, D.; García-García, A.; Sánchez-Gaytán, B.L.; Serrano-de la Rosa, L.E.; Melendez, F.J.; Choquesillo-Lazarte, D.; Rodríguez-Diéguez, A.; Castro, M.E.; González-Vergara, E. Bis-Citrullinato Copper(II) Complex: Synthesis, Crystal Structure, and Non-Covalent Interactions. *Crystals* **2022**, *12*, 1386. [[CrossRef](#)]
61. Ramírez-Contreras, D.; Vázquez-Rodríguez, S.; García-García, A.; Noriega, L.; Mendoza, A.; Sánchez-Gaytán, B.L.; Melendez, F.J.; Castro, M.E.; González-Vergara, E. L-Citrullinato-Bipyridine and L-Citrullinato-Phenanthroline Mixed Copper Complexes: Synthesis, Characterization and Potential Anticancer Activity. *Pharmaceutics* **2024**, *16*, 747. [[CrossRef](#)] [[PubMed](#)]
62. Rodrigues, J.A.O.; de Oliveira Neto, J.G.; de Barros, A.O.d.S.; Ayala, A.P.; Santos-Oliveira, R.; de Menezes, A.S.; de Sousa, F.F. Copper (II): Phenanthroline Complexes with L-Asparagine and L-Methionine: Synthesis, Crystal Structure and in-Vitro Cytotoxic Effects on Prostate, Breast and Melanoma Cancer Cells. *Polyhedron* **2020**, *191*, 114807. [[CrossRef](#)]
63. Corona-Motolinia, N.D.; Martínez-Valencia, B.; Noriega, L.; Sánchez-Gaytán, B.L.; Mendoza, A.; Meléndez-Bustamante, F.J.; Castro, M.E.; González-Vergara, E. Ternary Copper Complex of L-Glutamine and Phenanthroline as Counterions of Cyclo-Tetranadate Anion: Experimental-Theoretical Characterization and Potential Antineoplastic Activity. *Metals* **2021**, *11*, 1541. [[CrossRef](#)]
64. Shao, Y.; Molnar, L.F.; Jung, Y.; Kussmann, J.; Ochsenfeld, C.; Brown, S.T.; Gilbert, A.T.B.; Slipchenko, L.V.; Levchenko, S.V.; O'Neill, D.P. Advances in Methods and Algorithms in a Modern Quantum Chemistry Program Package. *Phys. Chem. Chem. Phys.* **2006**, *8*, 3172–3191. [[CrossRef](#)]
65. Balawender, R.; Geerlings, P. DFT-Based Chemical Reactivity Indices in the Hartree-Fock Method. II. Fukui Function, Chemical Potential, and Hardness. *J. Chem. Phys.* **2005**, *123*, 124103. [[CrossRef](#)]
66. Frisch, M.J.; Trucks, G.W.; Schlegel, H.B.; Scuseria, G.E.; Robb, M.A.; Cheeseman, J.R.; Scalmani, G.; Barone, V.; Petersson, G.A.; Nakatsuji, H.; et al. *Gaussian 16, Revision B.01*; Gaussian, Inc.: Wallingford, CT, USA, 2016.
67. Morris, G.M.; Goodsell, D.S.; Halliday, R.S.; Huey, R.; Hart, W.E.; Belew, R.K.; Olson, A.J. Automated Docking Using a Lamarckian Genetic Algorithm and an Empirical Binding Free Energy Function. *J. Comput. Chem.* **1998**, *19*, 1639–1662. [[CrossRef](#)]
68. Thomsen, R.; Christensen, M.H. MolDock: A New Technique for High-Accuracy Molecular Docking. *J. Med. Chem.* **2006**, *49*, 3315–3321. [[CrossRef](#)]
69. Fraser, B.J.; Beldar, S.; Seitova, A.; Hutchinson, A.; Mannar, D.; Li, Y.; Kwon, D.; Tan, R.; Wilson, R.P.; Leopold, K.; et al. Structure and Activity of Human TMPRSS2 Protease Implicated in SARS-CoV-2 Activation. *Nat. Chem. Biol.* **2022**, *18*, 963–971. [[CrossRef](#)]
70. Word, J.M.; Lovell, S.C.; Richardson, J.S.; Richardson, D.C. Asparagine and Glutamine: Using Hydrogen Atom Contacts in the Choice of Side-Chain Amide Orientation. *J. Mol. Biol.* **1999**, *285*, 1735–1747. [[CrossRef](#)]
71. Bitencourt-Ferreira, G.; de Azevedo, W.F. Molegro Virtual Docker for Docking. In *Docking Screens for Drug Discovery*; Humana: New York, NY, USA, 2019; pp. 149–167.
72. Heberle, G.; de Azevedo, W.F. Bio-Inspired Algorithms Applied to Molecular Docking Simulations. *Curr. Med. Chem.* **2011**, *18*, 1339–1352. [[CrossRef](#)]
73. Dias, R.; de Azevedo, W., Jr. Molecular Docking Algorithms. *Curr. Drug Targets* **2008**, *9*, 1040–1047. [[CrossRef](#)] [[PubMed](#)]
74. Nelder, J.A.; Mead, R. A Simplex Method for Function Minimization. *Comput. J.* **1965**, *7*, 308–313. [[CrossRef](#)]
75. Verdonk, M.L.; Cole, J.C.; Hartshorn, M.J.; Murray, C.W.; Taylor, R.D. Improved Protein-Ligand Docking Using GOLD. *Proteins Struct. Funct. Bioinform.* **2003**, *52*, 609–623. [[CrossRef](#)]

**Disclaimer/Publisher's Note:** The statements, opinions and data contained in all publications are solely those of the individual author(s) and contributor(s) and not of MDPI and/or the editor(s). MDPI and/or the editor(s) disclaim responsibility for any injury to people or property resulting from any ideas, methods, instructions or products referred to in the content.